Improved Sliding Mode Control for a Robotic Manipulator With Input Deadzone and Deferred Constraint

Yu Zhang, *Student Member, IEEE*, Linghuan Kong, *Member, IEEE*, Shuang Zhang, *Member, IEEE*, Xinbo Yu, *Member, IEEE*, and Yu Liu, *Senior Member, IEEE*

***Abstract*—In this article, neural network (NN)-based sliding mode control schemes are proposed for an n-link robotic manipulator with system uncertainties, input deadzone, and external perturbations. A novel error-shifting function is proposed to release initial conditions. NNs are employed to approximate the unknown parameters of both system uncertainties and input deadzone. To update the sliding mode scheme, two advanced sliding mode surfaces with error-shifting function and barrier function are proposed to reduce the dependency of prior information and to realize a finite time convergence result, collectively. It should be pointed out that the proposed methods do not require initial states to satisfy the prescribed constraint caused by the barrier function and can be applied under unknown initial conditions. Furthermore, finite-time convergence for both tracking errors and NN weights is guaranteed. The effectiveness of the proposed schemes is demonstrated by simulation and experiments on the KINOVA robot.**

***Index Terms*—Adaptive sliding mode control (SMC), barrier Lyapunov function (BLF), deferred performance constraints, neural networks (NNs), robotic manipulator.**

I. Introduction

RECENTLY, tracking problems of nonlinear systems with performance constraints have been researched [1], [2], [3]. It is common to deal with performance constraints with barrier Lyapunov function (BLF), which would approach infinity whenever its arguments are approaching the prescribed bounds. In [4], an integral BLF (IBLF) was proposed to satisfy input saturation and performance constraints. An adaptive control method with the neural networks (NNs) was utilized to improve approximation capability and adaptability. In [5], adaptive NNs and BLFs were applied to deal with unknown deadzone function and to meet performance constraints, respectively. It should be noted that the aforementioned researches based on BLFs require initial states to satisfy the prescribed constraints. It is very difficult to meet the initial constraint in real environments. Accordingly, a shift function was initially proposed in [6], and the delay constraints on the states were fulfilled by integrating this with barrier functions. In a subsequent study, detailed in [7], the shift function was employed in conjunction with impedance control to address the issue of the initial following force not meeting the constraint in the context of human-robot co-transportation. The methods in [8] extends the framework of [6] by incorporating an event-triggered mechanism, a strategic enhancement aimed at conserving computational resources. However, the aforementioned methods are exclusively applicable within the backstepping-based framework. In contrast, this article introduces a more generalized framework. This novel approach satisfies the delay constraint through the utilization of a novel proposed error-shifting function, and a deferred performance is realized within finite time.

Sliding mode control (SMC) is one of the techniques that has been adopted in various adaptive BLF-based methods to satisfy performance constraints due to its fast response and insensitivity to external disturbances and parameter variations [9], [10], [11], [12]. There are many drawbacks in tradition SMC, such as uncertain setting time and singular problem. Thus, nonsingular terminal SMC (NTSMC) [13] and nonsingular fast terminal SMC (NFTSMC) [14] have been proposed to realize finite-time convergence without singular points. Compared with NTSMC, a nonlinear term has been added in nonsingular fast terminal sliding mode surface to accelerate convergence rates. Many SMC-based methods satisfy the requirements of constraints and guarantee asymptotic convergence by entrapping sliding surfaces into BLFs directly, and thus the sliding surfaces are constrained in reaching phase. In [15], a variable structure via NTSMC with a novel guidance

Manuscript received 17 May 2023; accepted 20 July 2023. Date of publication 23 August 2023; date of current version 20 November 2023. This work was supported in part by the National Natural Science Foundation of China under Grant 61873297; in part by the China Postdoctoral Science Foundation under Grant 2018M630074; in part by the Guangdong Basic and Applied Basic Research Foundation under Grant 2020B1515120071; and in part by the Fundamental Research Funds for the China Central Universities under Grant FRF-GF-18-027B. This article was recommended by Associate Editor L. Chen. *(Corresponding author: Shuang Zhang.)*

Yu Zhang is with the Department of Computation, Information and Technology, Technical University of Munich, 85748 Garching, Germany (e-mail: zy.zhang@tum.de).

Linghuan Kong is with the Department of Electrical and Computer Engineering, Faculty of Science and Technology, University of Macau, Macau, China (e-mail: kong.ahuan@gmail.com).

Shuang Zhang and Xinbo Yu are with the School of Intelligence Science and Technology, the Institute of Artificial Intelligence, and the Key Laboratory of Perception and Control of Intelligent Bionic Unmanned System, Ministry of Education, University of Science and Technology Beijing, Beijing 100083, China (e-mail: zhangshuang.ac@gmail.com; yuxinbo17@qq.com).

Yu Liu is with the School of Automation Science and Engineering, South China University of Technology, Guangzhou 510640, China (e-mail: auylau@scut.edu.cn).

Color versions of one or more figures in this article are available at https://doi.org/10.1109/TSMC.2023.3301662.

Digital Object Identifier 10.1109/TSMC.2023.3301662

law was proposed to satisfy state constraints. In [16], barrier functions were entrapped into sliding mode surface to satisfy the error constraints. Although the reaching phase-based schemes have simple control structure, the steady errors are not constrained by barrier function directly and finite-time convergence is also hard to meet. In this article, the BLFs become a term of sliding surfaces in sliding phase, which means less steady tracking errors than BLFs designed in reaching phase and the nonlinear system is semiglobal practical finite time stable (SGPFTS).

The control laws based on SMC usually contain two components, including equivalent control and switching control. Specifically, the equivalent control is utilized to cope with system nonlinearities and to force the system states to reach the sliding phase from the reaching phase. The switching control is responsible for tackling the external disturbances, system uncertainties and maintaining the system states on the sliding phase. The harmful chattering is existence in the switching control due to the sign function [17]. Up to now, many useful methods are introduced to reduce chattering phenomenon. The boundary layer is one technique to remove the chattering phenomenon, but the better-chattering removal performances cause steady state errors [18]. High-order SMC is another technique to avoid chattering problem [17]. The switching control based on sliding surface is entrapped into high-derivative controller so that the input torques are continuous. But the complex calculation of high-order differential information increases implementation and time costs in practice, and thus some simple methods, degrading finite-time stability, are proposed to eliminate or attenuate chattering, including feedback linearization scheme [19], continuous full-order SMC [20], and observer strategy [21]. In this article, a mathematic technique is introduced to attenuate the issue of chattering, and the tracking errors will converge to a neighborhood region of zero.

Compensations of input nonlinearities are also essential to restrain control systems from decreasing systemic performances and to maintain precise motion. For tracking the desired trajectory accurately, some pioneering works have been developed to reduce nonlinear effects [22], [23], [24]. It is worth pointing out that artificial NNs were widely utilized for nonlinear systems because of their good approximation performance [25], [26], [27]. First of all, NN-based control methods have been proven that they require less information of nonlinear system dynamics to achieve the same control objectives. In [28], a prescribed tracking objective was met based on radial basis function (RBF) networks, which were utilized to cope with the uncertainties on robot systems. In [29], the uncertainties of a car-like wheeled robot were approximated by adopting RBF and thus a navigation system was developed. Second, NN-based approaches have acted as an effective deadzone approximation technique for nonlinear systems. In [30], two RBF neural networks (RBFNNs) were utilized to cope with the unknown width and slope of deadzone functions and to deal with the unknown dynamics of the robot, respectively. In [31], a flatted NN structure based on RBF with incremental learning was developed to compensate the nonlinearities of deadzone functions and to estimate system uncertainties. Finally, due to the outstanding approximation properties of NNs and the good transient performance of SMC, plenty of NNs-based control schemes are introduced via sliding mode. In [32], the fuzzy NNs were combined with the traditional SMC method to deal with structured and unstructured uncertainties. In [33], an NNs-based SMC scheme with a disturbance observer was proposed to compensate unknown nonlinear terms and input disturbances.

Motivated from the above analysis, we design adaptive NN-based control schemes with sliding mode technique. Fewer prior information is used while the benefits of advanced control methods are adopted to address system uncertainties, input nonlinearities and external perturbations. The main contributes of this article are as follows.

1) For the robotic manipulator, less prior information is needed than existing methods. A novel error-shifting function is proposed, and thus the introduced method does not rely on the initial conditions of system.
2) Smaller steady-state errors are produced because barrier functions and novel error shifting functions are entrapped into advanced SMC in the sliding phase instead of the reaching phase.
3) The chattering phenomenon is successfully attenuated without losing the convergence speed. By introducing a mathematic technique, an NN-based sliding mode strategy is developed to cope with system uncertainties and deadzone nonlinearities. The advantages of both SMC and NNs are remained and the chattering from the switching control law is reduced.

The remainder of this article is organized as follows. Section II states the formulated problem and main preliminaries of this article. Section III introduces the adaptive NTSMC and NFTSMC algorithms. In Section IV, simulation results verify the effectiveness of the proposed methods.

Notations: I_n and $\mathbb{R}$ denote the identity matrix in the space $\mathbb{R}^{n\times n}$ and the set of real number, respectively. $|\cdot|$ denotes the absolute value for scalars, $(\cdot)^{\mathrm{T}}$ is the transpose of a vector, and $||\cdot||$ implies the Euclidean norm for vectors and induced norm for matrices.

II. Problem Formulation

A. Preliminaries

In this article, we consider an n-link robotic system described by [34]

$$M(q)\ddot{q} + C(q,\dot{q})\dot{q} + G(q) + f_{\mathrm{dis}}(t) = D(\tau) \tag{1}$$

where $q, \dot{q}, \ddot{q} \in \mathbb{R}^n$ represent the position, velocity and acceleration vectors, $G(q) \in \mathbb{R}^n$ denotes the gravitational forces, $C(q,\dot{q}) \in \mathbb{R}^{n\times n}$ represents the coriolis and centrifugal matrix, $M(q) \in \mathbb{R}^{n\times n}$ denotes the positive-definite quality inertial matrix, the external disturbances are denoted by $f_{\mathrm{dis}}(t) \in \mathbb{R}^n$. Moreover, $\tau \in \mathbb{R}^n$ is the joint torques supplied by the actuators, and $D(\tau)$ is the deadzone function.

Property 1 [35]: The inertial matrix $M(q)$ is symmetric and positive definite.

Property 2 [36]: We assume $\bar{M}$, $\bar{C}$, and $\bar{G}$ are some positive constants. The matrices $M(q)$, $C(q,\dot{q})$ and $G(q)$ are

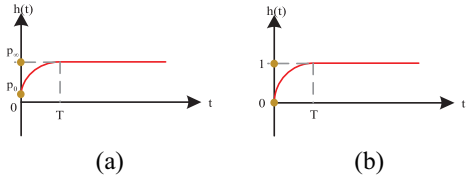

Fig. 1. Error-shifting function. (a) Original error-shifting function. (b) Error-shifting function with $p_0 = 0$ and $p_\infty = 1$.

upper bounded, i.e., $\|M(q)\| \leq \bar{M}$, $\|C(q,\dot{q})\| \leq \bar{C}\|\dot{q}\|$, and $\|G(q)\| \leq \bar{G}$.

Assumption 1 [36]: We assume that the inertial matrix is composed of the following parts:

$$M(q) = M_0(q) + \Delta M(q) \tag{2}$$

where $M_0(q)$ denotes the nominal part, and $\Delta M(q)$ stands for the uncertain part.

Property 3 [36]: The matrix $\Delta M(q)$ is upper bounded, i.e.,

$$\|\Delta M(q)\| \leq M_M \tag{3}$$

where M_M is a positive constant.

The deadzone nonlinearity can be expressed as [5]

$$D(\tau) = \begin{cases} O_r(\tau - d_r), & \tau \geq d_r \\ 0, & d_l < \tau < d_r \\ O_l(\tau - d_l), & \tau \leq d_l \end{cases} \tag{4}$$

where τ denotes the nominal control input, d_l and d_r denote unknown deadzone spacing, $O_r(\cdot)$ and $O_l(\cdot)$ are unknown smooth functions.

The control objective is to present an adaptive law to ensure that all the tracking errors satisfy the performance constraints and guarantee finite-time convergence under unknown initial conditions. To release requirements of initial state information, we introduce a novel error-shifting function

$$h(t) = \begin{cases} 1 - p_1, & 0 \leq t < T \\ 1, & T \leq t \end{cases} \tag{5}$$

where $p_1 = -3a([T^4/16](t + [T/2]) - [T^2/6](t - [T/2])^3 + ([(t - [T/2])^5]/5)) + b$, $a = (10/T^5)(p_\infty - p_0)$, $b = 1 - p_0 + 1.375(p_\infty - p_0)$, $p_0 = 0$, $p_\infty = 1$, and the preassigned time is $T > 0$. It is easily derived that $h(t)$ has the following properties.

1) $h(0) = 0$. When $t \in [0, T)$, $h(t)$ is smoothly increasing.
2) $h(T) = 1$ is its maximum value. When $\forall t \geq T$, $h(t)$ remains at such value.
3) $h(t)$ has continuous derivatives up to two-order. $\dot{h}(t)$ and $\ddot{h}(t)$ are known and bounded for all $t \in [0, \infty)$.

Remark 1: Actually, p_0 and p_∞ are also user-defined parameters, which is shown in Fig. 1. When we choose different value of these parameters, the function described as (5) keeps continuous up to two-order, which avoids singular problems in different control tasks. In this article, we choose $p_0 = 0$ and $p_\infty = 1$ to achieve control objectives.

The following assumptions help the subsequent analyses along as follows.

Assumption 2 [5]: We suppose that the disturbance f_{dis} is bounded. In other words, there exists an unknown constant $f \in \mathbb{R}^+$, so that $\|f_{\text{dis}}\| \leq f$ $\forall t \in [0, \infty)$.

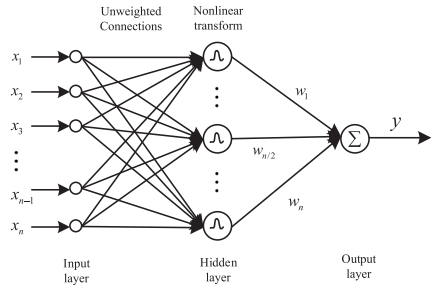

Fig. 2. Structure of RBF networks.

Assumption 3 [37]: The desired trajectory x_d is known, bounded and continuous.

Assumption 4 [37]: The parameters of deadzone function, d_r and d_l, are unknown constants. The conditions of $d_r > 0$ and $d_l < 0$ are met.

B. Function Approximation

RBF networks are utilized widely for approximating unknown function because of faster learning speed and high-quality approximate results [38]. A RBFNN is constituted of three layers, including the input layer, the hidden layer, and the output layer. Based on weightless connections, the main function of the input layer is to pass its environmental information to the hidden layer. The hidden layer contains lots of nodes, these information then is transformed nonlinearly by using a RBF like the Gaussian function, and finally pass to the output layer that is linear and acts as a summation unit. The structure of RBF is shown in Fig. 2.

The process for approximating the continuous function by utilizing linearly parameterized NNs can be represented by the following relation:

$$\begin{aligned} &y_i(X) : \mathbb{R}^q \to \mathbb{R} \\ &y_i(X) = W_i^T S_i(X), \quad i = 1, 2, \ldots, n \end{aligned} \tag{6}$$

where $X = [X_1, X_2, \ldots, X_q]^T \in \Omega_X \subset \mathbb{R}^q$ is input vector, $\iota > 1$ is the NN node number and $W_i \in \mathbb{R}^\iota$ is the weight vector. Based on numerous studies, if ι is prespecified largely, $y_i(X)$ can approximate any continuous function with acceptable errors. The approximation results are expressed as

$$y_i(X) = W_i^{*T} S_i(X) + \varepsilon_i(X) \tag{7}$$

where $\forall X \in \Omega_X \subset \mathbb{R}^q$, $\varepsilon_i(X)$ is the approximation error and is bounded, i.e., $|\varepsilon_i(X)| \leq \bar{\varepsilon}_i, i = 1, 2, \ldots, n$ $\forall X \in \Omega_X$, $\bar{\varepsilon}_i$ is a positive constant, W_i^{*T} is the ideal weight vector and is utilized to minimize $|\varepsilon_i(X)|$ for all $X \in \Omega_X \subset \mathbb{R}^q$, i.e.,

$$W_i^* = \arg \min_{W_i \in R^\iota} \left\{ \sup_{X \in \Omega_X} \left| y_i(X) - W_i^T S_i(X) \right| \right\} \tag{8}$$

where $s_j(X)$ is Gaussian function, i.e.,

$$s_j(X) = \exp\left[\frac{-(X - \mu_j)^T (X - \mu_j)}{\eta_j^2} \right], \quad j = 1, 2, \ldots, \iota$$

and η_j is the width of $s_j(X)$. In the receptive field, the center is $\mu_j = [\mu_{j1}, \mu_{j2}, \ldots, \mu_{kq}]^{\mathrm{T}}$.

C. Technical Lemmas and Definitions

Definition 1 [39]: For a nonlinear system $\dot{g}(t) = h(g(t))$, if there exists σ, ε and convergence time $t_r(\sigma, g_0) < \infty$ to make $||g(t)|| < \varepsilon$ for all $g(t_0) = g_0$ and $t \geq t_0 + t_r$. Then, the equilibrium $g = 0$ of the nonlinear system is SGPFTS.

Lemma 1 [39]: Consider the nonlinear system $\dot{g}(t) = h(g(t))$, $h(0) = 0$, and $g(t) \in \mathbb{R}^n$. Suppose there exists a positive-definite function $L(g(t))$ such that

$$\dot{L}(g) \leq -\alpha L(g)^{\beta} + \sigma, t \geq 0 \tag{9}$$

where $\alpha > 0$, $0 < \beta < 1$, and $\sigma > 0$. And the nonlinear system is SGPFTS.

The finite time t_r is shown as

$$t_r = \frac{1}{(1-\beta)\varpi\alpha}\left(L(g(0))^{1-\beta} - \left(\frac{\sigma}{(1-\varpi)\alpha}\right)^{\frac{(1-\beta)}{\beta}}\right) \tag{10}$$

where $0 < \varpi < 1$.

Lemma 2 [40]: For $U_i, i = 1, 2, \ldots, n$, if $0 < \gamma < 1$, then following inequality holds:

$$(|U_1| + |U_2| + \cdots + |U_n|)^{\gamma} \leq |U_1|^{\gamma} + \cdots + |U_n|^{\gamma}. \tag{11}$$

Lemma 3 [5]: The basis function of the Gaussian RBFNN with $\hat{X} = X - \gamma\psi$ being the input vector, where ψ is a bounded vector and γ is a positive constant given as

$$s_k\left(\hat{X}\right) = \exp\left[\frac{-\left(\hat{X}-\mu_k\right)^T\left(\hat{X}-\mu_k\right)}{\eta_k{}^2}\right], \quad k = 1, 2, \ldots, \iota$$
$$S\left(\hat{X}\right) = S(X) + \gamma S_t \tag{12}$$

where S_t is a bounded vector function.

Lemma 4 [14]: When a sliding surface reaches the origin, the moving point reaches the sliding surface. Thus, the system states are changed from the reaching phase to the sliding phase. The convergence times t_m and t_n of the sliding modes are determined by the equations: $0 = e + \chi^{-1}\text{sig}^{a/b}(\dot{e})$ and $0 = e + \delta^{-1}\text{sig}^{\theta}(e) + \chi^{-1}\text{sig}^{a/b}(\dot{e})$. Then the finite time t_m and t_n make $e(t)$ reach the origin given as follows:

$$t_m = \max_{1\leq i\leq n}\left\{\frac{a}{(\chi_i)^{\frac{a}{b}}(a-b)}|e_i(t_0+t_r)|^{\frac{(a-b)}{b}}\right\} \tag{13}$$

where t_0 is the initial time and t_r is the time horizon of reaching time. $\chi^{-1} = \text{diag}\{\chi_1^{-1}, \ldots, \chi_n^{-1}\} \in \mathbb{R}^{n\times n}$ is a positive-definite matrix, a and b are positive odd constraints satisfying the relation $1 < a/b < 2$, and $\text{sig}^{a/b}(\dot{e}) = [|\dot{e}_1|^{a/b}\text{sign}(\dot{e}_1), \ldots, |\dot{e}_n|^{a/b}\text{sign}(\dot{e}_n)]^{\text{T}} \in \mathbb{R}^n$

$$t_n = \max_{1\leq i\leq n}\left\{\frac{1}{\chi_i^{\frac{a}{b}}}\int_o^{|e_i(t_0+t_r)|}\frac{1}{\left(\upsilon-\delta_i^{-1}\upsilon^{\theta}\right)^{\frac{a}{b}}}d\upsilon\right\} \tag{14}$$

where $\theta > a/b$, $\delta^{-1} = \text{diag}\{\delta_1^{-1}, \ldots, \delta_n^{-1}\} \in \mathbb{R}^{n\times n}$ and $\text{sig}^{\theta}(e) = [|e_1|^{\theta}\text{sign}(e_1), \ldots, |e_n|^{\theta}\text{sign}(e_n)]^{\text{T}}$.

Lemma 5: Let b be a positive real number, and if $o(y) > 0$ is any real valued function

$$|y|^b \leq (1-b)|b|^{\frac{b}{1-b}} + |y|. \tag{15}$$

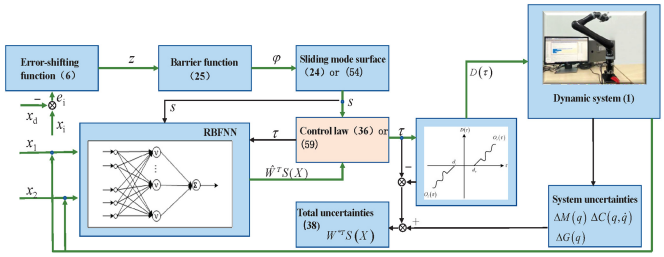

Fig. 3. Structure of NN-based sliding mode strategy.

Proof: If a and b are any positive real numbers, based on Young's inequality

$$cd \leq \frac{c^{\gamma}}{\gamma} + \frac{(\gamma-1)d^{\gamma/(\gamma-1)}}{\gamma}, \gamma > 1, c \geq 0, d \geq 0 \tag{16}$$

with

$$c = o^{a/(a+b)}, d = |y|^b o^{-a/(a+b)}, \gamma = \frac{a+b}{a}. \tag{17}$$

Based on (16) and (17), we have

$$|y|^b \leq \frac{a}{a+b}o(y) + \frac{b}{a+b}o^{-a/b}(y)|y|^{a+b}. \tag{18}$$

Then, if $a = 1-b$ and $o(y) = b^{(b/[1-b])}$, the following result is:

$$|y|^b \leq (1-b)|b|^{\frac{b}{1-b}} + |y|. \tag{19}$$

■

III. Control Design

In this part, we design the control schemes based on a novel nonsingular terminal sliding mode surface and a novel nonsingular fast terminal sliding mode surface. The control objectives are summarized in the following three aspects.

1) The proposed control laws do not need any precise-prior information of the robotic systems, including initial state conditions, gain functions, and the width and slope of deadzone functions.
2) The proposed schemes can be implemented when tracking errors violate the prescribed constraints initially, which are different from other BLF-based schemes.
3) The prescribed constraints are achieved within finite time and the arguments of unknown functions remain within a compact set, on which the NN approximation is valid.

The structure of the proposed NN-based sliding mode approach of this section is shown in Fig. 3.

A. Nonsingular Terminal Sliding-Mode Control Design

First, an NN-based NTSMC strategy is proposed based on (1) and (2). Let $x_1 = [q_1, q_2, \ldots, q_n]^{\text{T}}$ and $x_2 = [\dot{q}_1, \dot{q}_2, \ldots, \dot{q}_n]^{\text{T}}$, the state space model of the robot dynamics is written as

$$\dot{x}_1 = x_2$$
$$\dot{x}_2 = M_0^{-1}\left[D(\tau) - C(x_1, x_2) - G(x_1) - f_{\text{dis}} - \Delta M\ddot{q}\right]. \tag{20}$$

The generalized tracking error is defined as

$$e = x_1 - x_d. \tag{21}$$

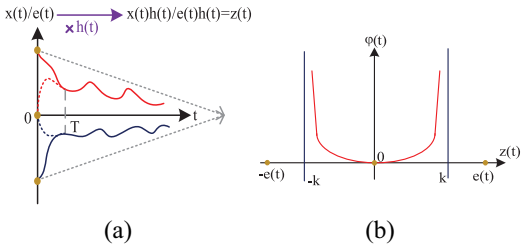

(a) (b)

Fig. 4. Role of error-shifting function. (a) Original and shifted state/error evolution within prescribed time T. (b) Barrier function (24).

In order to release the initial conditions for robotic system, we transform the tracking error into a new variable as

$$z = h(t)e. \tag{22}$$

Remark 2: According to the error-shifting transformation $h(t)$, the initial transferable error z reaches the origin whatever the values of the initial tracking error e are. Based on the properties of the error-shifting transformation, the transferable error is transferred into the real tracking error after the preassigned time T.

For achieving the control objectives within finite time in sliding phase, a novel nonsingular terminal sliding mode surface is constructed as

$$s = \varphi + \beta^{-1}\text{sig}^{\frac{p}{q}}(\dot{\varphi}) \tag{23}$$

where $s = [s_1, \ldots, s_n]^{\mathrm{T}} \in \mathbb{R}^n$ is the sliding variable, $\beta^{-1} = \text{diag}\{\beta_1^{-1}, \ldots, \beta_n^{-1}\} \in \mathbb{R}^{n\times n}$ is a positive-definite matrix, p and q are positive constants satisfying $1 < (p/q) < 2$, $\varphi = [\varphi_1, \ldots, \varphi_n]^T \in \mathbb{R}^n$ is the vector of barrier functions and $\text{sig}^{(p/q)}(\dot{\varphi}) = [|\dot{\varphi}_1|^{(p/q)}\text{sign}(\dot{\varphi}_1), \ldots, |\dot{\varphi}_n|^{(p/q)}\text{sign}(\dot{\varphi}_n)]^{\mathrm{T}} \in \mathbb{R}^n$.

The barrier function, φ_i, $i = 1, 2, \ldots, n$, is defined as

$$\varphi_i = \frac{1}{2}\ln\frac{k^2}{k^2 - z_i^2} \tag{24}$$

where k is the prescribed constraint.

Differentiating φ_i with respect to time, we have

$$\dot{\varphi}_i = \frac{z_i\dot{z}_i}{k^2 - z_i^2}. \tag{25}$$

Differentiating (25) with respect to time leads to

$$\ddot{\varphi}_i = \sum_{i=1}^{n}\frac{\dot{z}_i^2\left(z_i^2 + k^2\right)}{\left(k^2 - z_i^2\right)^2} + \sum_{i=1}^{n}\frac{z_i}{k^2 - z_i^2}\ddot{z}_i. \tag{26}$$

Remark 3: In (24), we introduce a universal symmetric barrier function to provide a symmetric constraint requirement. When the initial tracking error e violates the prescribed bound k, the traditional BLFs cannot work [4], [41]. By utilizing (22), the transformed error variable z is switched to zero in the initial time and then returns to e after a preassigned time T. With this setup, the constructed BLF will be well-defined initially and a deferred constraint is realized. Therefore, the proposed sliding surface can be implemented to address performance constraints under unknown initial conditions. The main function of the error-shifting transformation is shown in Fig. 4.

Differentiating s with respect to time, we have

$$\dot{s} = \dot{\varphi} + \beta^{-1}\frac{p}{q}\text{sig}^{\left(\frac{p}{q}\right)-1}(\dot{\varphi})\ddot{\varphi} \tag{27}$$

where $\text{sig}^{(p/q)-1}(\dot{\varphi}) = \text{diag}\{|\dot{\varphi}_1|^{(p/q)-1}, \ldots, |\dot{\varphi}_n|^{(p/q)-1}\}$.

Substituting (25) and (26) into (27), the following result is given as:

$$\dot{s} = \dot{\varphi} + \beta^{-1}\frac{p}{q}\text{sig}^{\left(\frac{p}{q}\right)-1}(\dot{\varphi})\Big(A_1 + A_2\Big(A_3 + h\Big(M_0^{-1}(\tau - \Delta\tau - C(x_1, x_2)x_2 - f_{\text{dis}} - \Delta M\ddot{q} - G(x_1)) - \ddot{x}_d\Big)\Big)\Big) \tag{28}$$

where $A_1 = [A_{11}, A_{12}, \ldots, A_{1n}] \in \mathbb{R}^n$, $A_{1i} = ([\dot{z}_i^2(z_i^2 + k^2)]/[(k^2 - z_i^2)^2])$, $i = 1, 2, \ldots, n$, $A_2 = \text{diag}\{A_{2i}\} \in \mathbb{R}^{n\times n}$, $A_{2i} = (z_i/[k^2 - z_i^2])$, $A_3 = \ddot{h}e + 2\dot{h}\dot{e}$, $D(\tau) = \tau - \Delta\tau$, and $\Delta\tau$ is the error of the ideal control input.

Control law then can be further proposed and it consists of two components, including equivalent control ($\tau_{eq}(t)$) and switching control ($\tau_{sw}(t)$). Their corresponding roles have already been described in the introductory section. For (28), the equivalent law can be chosen as

$$\tau_{eq} = \frac{M}{h}\left(A_2^{-1}\left(-\beta\frac{q}{p}\text{sig}^{2-\left(\frac{p}{q}\right)}(\dot{\varphi}) - A_1\right) - A_3 + h\ddot{x}_d\right) + \Delta\tau + C(x_1, x_2)x_2 + f_{\text{dis}} + G(x_1). \tag{29}$$

The switching control is given as

$$\tau_{sw} = \frac{M}{h}A_2^{-1}(-\eta\text{sign}(s)) \tag{30}$$

where η is a known positive constant, and

$$\text{sig}^{2-\left(\frac{p}{q}\right)}(\dot{\varphi}) = \Big[|\dot{\varphi}_1|^{2-\left(\frac{p}{q}\right)}\text{sign}(\dot{\varphi}_1), \ldots, |\dot{\varphi}_n|^{2-\left(\frac{p}{q}\right)}\text{sign}(\dot{\varphi}_n)\Big]^{\mathrm{T}} \in \mathbb{R}^n. \tag{31}$$

Substituting (29) and (30) into (28) results in

$$\dot{s} = \dot{\varphi} + \beta^{-1}\frac{p}{q}\text{sig}^{\left(\frac{p}{q}\right)-1}(\dot{\varphi})\left(-\eta\text{sign}(s) - \beta\frac{q}{p}\text{sig}^{2-\left(\frac{p}{q}\right)}(\dot{\varphi})\right) = -\beta^{-1}\frac{p}{q}\text{sig}^{\left(\frac{p}{q}\right)-1}(\dot{\varphi})\eta\text{sign}(s). \tag{32}$$

Because the parameters of $\Delta\tau$, M, G, $G(x_1, x_2)x_2$ are unknown, the control law (29) and (30) are unavailable. Therefore, a RBFNN is utilized to approximate these unknown parameters in this article. We propose NN-based control law as

$$\tau_{eq} = \frac{M_0}{h}\left(A_2^{-1}\left(-\beta\frac{q}{p}\text{sig}^{2-\left(\frac{p}{q}\right)}(\dot{\varphi}) - A_1\right) - A_4 - A_3 + h\ddot{x}_d\right) \tag{33}$$

where $A_4 = \mu_2^2h^2(M_0^{-1})^2\beta^{-1}(p/q)\text{sig}^{(p/q)-1}(\dot{\varphi})A_2s \in \mathbb{R}^n$, and μ_2 is a positive constant. Switching control is

$$\tau_{sw} = -\frac{\eta M_0}{h}A_2^{-1}s + \hat{W}^TS(X). \tag{34}$$

Based on (33) and (34), the actual control law based on NTSMC is then introduced as

$$\tau_1 = \tau_{eq} + \tau_{sw}. \tag{35}$$

Network updating law is designed as

$$\dot{\hat{W}}_i = -\Gamma_{1i}\left[s_i^T Q_i S_i(X) + \sigma_i \hat{W}_i\right] \tag{36}$$

where $Q = \beta^{-1}(p/q)\mathrm{sig}^{(p/q)-1}(\dot{\varphi})A_2 h M_0^{-1} \in \mathbb{R}^{n\times n}$, $\Gamma_{1i}, i = 1, 2, \ldots, n$, are real, symmetric and positive-definite constant gain matrix, $\hat{W}^T S(X)$ is used to approximate $W^{*T}S(X)$, which is given as

$$W^{*T}S(X) = C(x_1, x_2)x_2 + G(x_1) + \Delta M\ddot{q} + \Delta\tau - \epsilon \tag{37}$$

where W^{*T} is the ideal weights, ϵ is approximation errors of the NN and $X = [x_1^{\mathrm{T}}, x_2^{\mathrm{T}}, \tau_1^{\mathrm{T}}, s^{\mathrm{T}}]^{\mathrm{T}}$.

Remark 4: Obviously, the model-based switching control (30) relies on sign function, which causes chattering problem. Therefore, a mathematic transformation based on Lemma 5 has been introduced to reduce this chattering. The relative detail will be reflected in (46), (47) and (48).

Considering (37), and substituting (35) into (28), we obtain

$$\begin{aligned}\dot{s} = &-\eta\beta^{-1}\frac{p}{q}\mathrm{sig}^{\left(\frac{p}{q}\right)-1}(\dot{\varphi})s - A_6 + \beta^{-1}\frac{p}{q}\mathrm{sig}^{\left(\frac{p}{q}\right)-1}(\dot{\varphi})\\ &\times A_2 h M_0^{-1}\left(\tilde{W}^T S(X) - \epsilon - f_{\mathrm{dis}}\right)\end{aligned} \tag{38}$$

where $\tilde{W}{=}\hat{W} - W^*$, and $A_6 = \beta^{-1}(p/q)\mathrm{sig}^{(p/q)-1}(\dot{\varphi})A_2A_4 \in \mathbb{R}^n$. Obviously, A_6 is a positive-definite matrix.

Theorem 1: For the system dynamics (1) with input deadzone (4) and external perturbations, the control law (35) with weight updating law (36) is proposed under Assumptions 1-4 to force the signals s, φ, $\dot{\varphi}$, and $\tilde{W}$ to be semiglobally uniformly bounded and remain within the compact sets Ω_s Ω_φ, $\Omega_{\dot{\varphi}}$, and Ω_w, respectively, defined by

$$\begin{aligned}\Omega_s &:= \left\{s \middle| \|s\| \le L_s = \sqrt{2}\left(\frac{\sigma}{(1-\varpi)\alpha_1}\right)^{1/2\iota}\right\}\\ \Omega_\varphi &:= \{\varphi_i \middle| |\varphi_i| \le 2L_s\},\ \Omega_w := \left\{\tilde{W} \middle| \left\|\tilde{W}\right\| \le L_s\right\}\\ \Omega_{\dot{\varphi}} &:= \left\{\dot{\varphi}_i \middle| |\dot{\varphi}_i| \le \left(\frac{1}{\beta_i}L_s\right)^{q/p}\right\}\end{aligned} \tag{39}$$

with $0 < \varpi < 1$, $\sigma = (1/2)\sum_{i=1}^n \sigma_i(W_i^{*T}W_i^* + 1) + (n+1)D$, and $\alpha_1 = \eta^{1/2}\Pi(\dot{\varphi})^{1/2}$.

Furthermore, the nonlinear system are stable under unknown initial conditions within finite time $t_\alpha = t_1 + t_2$, where

$$\begin{aligned}t_1 &= \frac{1}{(1-\iota)\varpi\alpha_1}\left(V\left(s(0), \tilde{W}(0)\right)^{1-\iota} - \left(\frac{\sigma}{(1-\varpi)\alpha_1}\right)^{\frac{(1-\iota)}{\iota}}\right)\\ t_2 &= \max_{1\le i\le n}\left\{\frac{p}{\frac{p}{(\beta_i)^q}(p-q)}|\varphi_i(t_0+t_1)|^{\frac{(p-q)}{q}}\right\}\end{aligned} \tag{40}$$

where $\iota = (1/2)$, the period $t_\eta \in [t_0, t_1]$ is the reaching phase, and the period $t_\mu \in [t_1, t_2]$ is the sliding phase.

Proof: For achieving the control objectives within finite time in reaching phase, consider the following Lyapunov function candidate:

$$V = \frac{1}{2}s^T s + \frac{1}{2}\sum_{i=1}^n \tilde{W}_i^T\Gamma_{1i}^{-1}\tilde{W}_i \tag{41}$$

where $\Gamma_{1i}^{-1}, i = 1, 2, \ldots, n$, are the inverse of the matrix Γ_{1i}.

Differentiating V with respect to time, we obtain

$$\dot{V} = s^T\dot{s} + \sum_{i=1}^n \tilde{W}_i^T\Gamma_{1i}^{-1}\dot{\hat{W}}_i. \tag{42}$$

Substituting (38) into (42) gives

$$\begin{aligned}\dot{V} = &-\sum_{i=1}^n \eta\beta^{-1}\frac{p}{q}\mathrm{sig}_i^{\left(\frac{p}{q}\right)-1}(\dot{\varphi})s_i^2 - s^{\mathrm{T}}A_6\\ &+ s^T Q\left(\tilde{W}^T S(X) - \epsilon - f_{\mathrm{dis}}\right) + \sum_{i=1}^n \tilde{W}_i^T\Gamma_{1i}^{-1}\dot{\hat{W}}_i.\end{aligned} \tag{43}$$

Then substituting (36) into (43), we have

$$\dot{V} \le -\eta\Pi(\dot{\varphi})\|s\|^2 - \sum_{i=1}^n \sigma_i\tilde{W}_i^T\hat{W}_i - s^T Q(\epsilon + f_{\mathrm{dis}}) - s^{\mathrm{T}}A_6 \tag{44}$$

where

$$\Pi(\dot{\varphi}) := \inf_{1<i<n}\left\{\left(\beta^{-1}\frac{p}{q}\mathrm{sig}^{\left(\frac{p}{q}\right)-1}(\dot{\varphi})\right)_i\right\}. \tag{45}$$

Based on Lemma 5, we obtain

$$-\left(\eta^{1/2}\Pi(\dot{\varphi})^{1/2}\|s\|\right)^2 \le -\left(\eta^{1/2}\Pi(\dot{\varphi})^{1/2}|s|\right) + D \tag{46}$$

$$-s^{\mathrm{T}}A_6 \le -\sum_{i=1}^n \mu_2 h\left(M_0^{-1}\right)\beta^{-1}\frac{p}{q}\mathrm{sig}_i^{\left(\frac{p}{q}\right)-1}(\dot{\varphi})|A_{2i}||s_i| + nD \tag{47}$$

$$-s^T Q\epsilon \le \sum_{i=1}^n |\epsilon_i|h\left(M_0^{-1}\right)\beta^{-1}\frac{p}{q}\mathrm{sig}_i^{\left(\frac{p}{q}\right)-1}(\dot{\varphi})|A_{2i}||s_i| \tag{48}$$

where $D = (1-b)|b|^{(b/[1-b])}$, $b = 1/2$. Furthermore, since $-\tilde{W}^T\hat{W} = -\tilde{W}^T(W^*+\tilde{W}) = -\tilde{W}^T\tilde{W} - \tilde{W}^T W^*$ and $-\tilde{W}^T W^* \le (1/2)(\tilde{W}^T\tilde{W} + W^{*T}W^*)$, we get $-\tilde{W}^T\hat{W} \le -(1/2)\tilde{W}^T\tilde{W} + (1/2)W^{*T}W^* \le -(\tilde{W}^T\tilde{W})^{(1/2)} + (1/2)(W^{*T}W^* + 1)$, and (44) is rewritten as

$$\begin{aligned}\dot{V} &\le -\eta^{1/2}\Pi(\dot{\varphi})^{1/2}\|s\| + \frac{1}{2}\sum_{i=1}^n \sigma_i\left(W_i^{*T}W_i^* + 1\right)\\ &\quad - \sum_{i=1}^n \sigma_i\left(\tilde{W}_i^T\tilde{W}_i\right)^{\frac{1}{2}} + (n+1)D\\ &\le -\alpha_1 V(x)^\iota + \sigma\end{aligned} \tag{49}$$

where $0 < \iota = (1/2) < 1$, $\|\mu_2\| \ge \|\epsilon\| + \|f_{\mathrm{dis}}\|$, $\alpha_1 > 0$ and $\sigma > 0$ are constants defined in (40). According to Definition 1, Lemmas 1–4, and (49), $V(S(0), \tilde{W}(0)) \le \sigma/(1-\varpi)\alpha_1$ for all $t \ge t_1$. Thus, s and $\tilde{W}$ converge to the region described as (39).

Because of $|s_i| \le L_s$, we obtain

$$\varphi_i + \beta^{-1}\mathrm{sig}_i^{\frac{p}{q}}(\dot{\varphi}) = \varsigma_i, \quad |\varsigma_i| \le L_s, \quad i = 1, 2, \ldots, n. \tag{50}$$

The (50) can be rewritten as

$$\varphi_i + \left(\beta_i^{-1} - \frac{\varsigma_i}{\mathrm{sig}_i^{\frac{p}{q}}(\dot{\varphi})}\right)\mathrm{sig}_i^{\frac{p}{q}}(\dot{\varphi}) = 0. \tag{51}$$

Based on Lemma 4, when $\beta_i^{-1} > (\varsigma_i/[\mathrm{sig}_i^{(p/q)}(\dot{\varphi})])$, (51) is also the form of NTSMC, and thus the barrier function will

converge to the set $|\dot{\varphi}_i| \leq ([1/\beta_i]L_s)^{q/p}$ within finite time. Furthermore, using dynamics (51), we can further obtain

$$|\varphi_i| \leq \beta_i^{-1}|\dot{\varphi}_i|^{\frac{p}{q}} + |\varsigma_i| \leq L_s + L_s = 2L_s. \tag{52}$$

Thus, s, φ, $\dot{\varphi}$ and $\tilde{W}$ converge to the set described as (39) and the finite time is given in (40). ■

Remark 5: In this article, the proposed error-shifting function is entrapped into barrier functions, and further combined with NN-based SMC in the sliding phase described in (23) and (41). If the proposed function is designed in the reaching phased, i.e., $s = e + \beta^{-1}\text{sig}^{(p/q)}(\dot{e})$ and $V = (1/2)\ln(k^2/[k^2 - s^T s])$, the steady errors meet the region $\|s\| < k$. Therefore, the proposed methods has smaller steady errors than the strategies in other reaching-phase-designed literatures due to $\|L_s\| < k$ by choosing suitable η.

B. Nonsingular Fast Terminal Sliding-Mode Control Design

In this section, for achieving the control objectives within finite time in sliding phase, we introduce the novel nonsingular terminal sliding mode surface

$$s_2 = \varphi + \alpha^{-1}\text{sig}^{\gamma}(\varphi) + \beta^{-1}\text{sig}^{\frac{p}{q}}(\dot{\varphi}) \tag{53}$$

where $\text{sig}^{p/q}(\dot{\varphi}) = [|\dot{\varphi}_1|^{p/q}\text{sign}(\dot{\varphi}_1), \ldots, |\dot{\varphi}_n|^{p/q}\text{sign}(\dot{\varphi}_n)]^{\text{T}}$, $s_2 \in \mathbb{R}^n$ is the sliding variable, p and q are positive constants satisfying the relation $1 < \frac{p}{q} < 2$ and $\gamma > \frac{p}{q}$, $\alpha^{-1} = \text{diag}\{\alpha_1^{-1}, \ldots, \alpha_n^{-1}\} \in \mathbb{R}^{n\times n}$ and $\beta^{-1} = \text{diag}\{\beta_1^{-1}, \ldots, \beta_n^{-1}\} \in \mathbb{R}^{n\times n}$ are positive-definite matrices, and $\text{sig}^{\gamma}(\varphi) = [|\varphi_1|^{\gamma}\text{sign}(\varphi_1), \ldots, |\varphi_n|^{\gamma}\text{sign}(\varphi_n)]^{\text{T}}$.

The following barrier function $\varphi_i, i = 1, 2, \ldots, n$, is similar to (24), (25) and (26).

Upon differentiating s_2 with respect to time, we have

$$\dot{s}_2 = \dot{\varphi} + \alpha^{-1}\gamma\text{sig}^{\gamma-1}(\varphi)\dot{\varphi} + \beta^{-1}\frac{p}{q}\text{sig}^{\left(\frac{p}{q}\right)-1}(\dot{\varphi})\ddot{\varphi} \tag{54}$$

where

$$\text{sig}^{\gamma-1}(\varphi) = \text{diag}\left\{|\varphi_1|^{\gamma-1}, \ldots, |\varphi_n|^{\gamma-1}\right\} \in \mathbb{R}^{n\times n}$$
$$\text{sig}^{\left(\frac{p}{q}\right)-1}(\dot{\varphi}) = \text{diag}\left\{|\dot{\varphi}_1|^{\left(\frac{p}{q}\right)-1}, \ldots, |\dot{\varphi}_n|^{\left(\frac{p}{q}\right)-1}\right\} \in \mathbb{R}^{n\times n}.$$

The deadzone function has been described as (4).

Remark 6: There may be initially excessive overload of input torque due to the term of $1/h$. But this phenomenon can also be addressed by choosing suitable p_0 in (5). For example, if we choose $p_0 = 0.05$, the initial transformed error also satisfies the barrier function (24) for some cases. Due to the novel error-shifting function is continuous, there is no singularity in control law and thus the proposed method is more flexible in application. Moreover, the proposed schemes for addressing input nonlinearity are similar to these literatures in [35], [42], [43], and [44].

Substituting (25) and (26) into (54), we have

$$\begin{aligned}\dot{s}_2 = \dot{\varphi} + \alpha^{-1}\gamma\text{sig}^{\gamma-1}(\varphi)\dot{\varphi} + \beta^{-1}\frac{p}{q}\text{sig}^{\left(\frac{p}{q}\right)-1}(\dot{\varphi}) \\ \times \Big(A_1 + A_2\Big(A_3 + h\Big(M_0^{-1}(\tau - \Delta M\ddot{q} - \Delta\tau \\ - C(x_1, x_2)x_2 - f_{\text{dis}} - G(x_1)) - \ddot{x}_d\Big)\Big)\Big)\end{aligned} \tag{55}$$

where the definition of A_1, A_2, and A_3 are defined in aforementioned section. Because $\Delta\tau$, M, G and $G(x_1, x_2)x_2$ are unknown vectors, a RBFNN will be used to approximate these parameters. We propose the actual equivalent controller as

$$\begin{aligned}\tau_{eq} = \frac{M_0}{h}\Bigg(A_2^{-1}\Bigg(-\alpha^{-1}\gamma\text{sig}^{\gamma-1}(\varphi)\beta\frac{q}{p}\text{sig}^{2-\left(\frac{p}{q}\right)}(\dot{\varphi}) \\ - \eta_1\text{sign}(s_2) - \beta\frac{q}{p}\text{sig}^{2-\left(\frac{p}{q}\right)}(\dot{\varphi}) - A_1\Bigg) \\ - A_5 - A_3 + h\ddot{x}_d\Bigg) + \hat{W}^T S(X)\end{aligned} \tag{56}$$

where η_1 is a known positive constant, $\text{sig}^{2-(q/p)}(\dot{\varphi})$ is defined in (31), $A_5 = \mu_2^2 h^2 (M_0^{-1})^2 \beta^{-1}(p/q)\text{sig}^{(p/q)-1}(\dot{\varphi})A_2 s_2 \in \mathbb{R}^n$, and the switching control law is designed as

$$\tau_{sw} = -\frac{\eta_1 M_0}{h}A_2^{-1}s_2 + \hat{W}^T S(X) \tag{57}$$

where the configuration of NN is the same as that in Section III-A, and $X = [x_1^{\text{T}}, x_2^{\text{T}}, \tau_2^{\text{T}}, s_2^{\text{T}}]^{\text{T}}$. The actual control law based on NFTSMC is

$$\tau_2 = \tau_{eq} + \tau_{sw} \tag{58}$$

and the updating law are described as

$$\dot{\hat{W}}_i = -\Gamma_{2i}\left[s_{2i}^T Q_i S_i(X) + \sigma_i \hat{W}_i\right] \tag{59}$$

and other parameters are defined in (37). Substituting (56) and (37) into (55), we have

$$\begin{aligned}\dot{s_2} = -\eta_1\beta^{-1}\frac{p}{q}\text{sig}^{\left(\frac{p}{q}\right)-1}(\dot{\varphi})s_2 + \beta^{-1}\frac{p}{q}\text{sig}^{\left(\frac{p}{q}\right)-1}(\dot{\varphi}) \\ \times A_2 h M_0^{-1}\left(\tilde{W}^T S(X) - \epsilon - f_{\text{dis}}\right) - A_7\end{aligned} \tag{60}$$

where $A_7 = \beta^{-1}(p/q)\text{sig}^{(p/q)-1}(\dot{\varphi})A_2 A_5 \in \mathbb{R}^n$. Obviously, the only difference between (38) and (60) is that s becomes s_2 and the algorithm structure is shown in Fig. 3.

Theorem 2: For the system dynamics suffering from input deadzone and external perturbations described by (1) and (4), respectively, under Assumptions 1-4, and the control law (58) with the adaptive law (59), the signals s_2, φ, $\dot{\varphi}$, and $\tilde{W}$ are semiglobally uniformly bounded and within the compact sets Ω_{s_2} Ω_{φ_2}, $\Omega_{\dot{\varphi}_2}$, and Ω_{w_2}, respectively, defined by

$$\begin{aligned}\Omega_{s_2} &:= \left\{s_2 \middle| \|s_2\| \leq L_{s_2} = \sqrt{2}\left(\frac{\sigma_1}{(1-\varpi)\alpha_2}\right)^{1/2t}\right\} \\ \Omega_{\varphi_2} &:= \left\{\varphi_i \middle| |\varphi_i| \leq 2L_{s_2}\right\} \\ \Omega_{\dot{\varphi}_2} &:= \left\{\dot{\varphi}_i \middle| |\dot{\varphi}_i| \leq \left(\frac{1}{\beta_i}L_{s_2}\right)^{q/p}\right\} \\ \Omega_{w_2} &:= \left\{\tilde{W} \middle| \|\tilde{W}\| \leq L_{s_2}\right\}\end{aligned} \tag{61}$$

with $0 < \varpi < 1$, $\sigma_1 = (1/2)\sum_{i=1}^n \sigma_i(W_i^{*T}W_i^* + 1) + (n+1)D$, and $\alpha_2 = \eta_1^{1/2}(\inf_{1<i<n}\{(\beta^{-1}(p/q)\text{sig}^{(p/q)-1}(\dot{\varphi}))_i\})^{1/2}$.

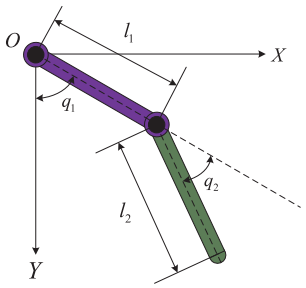

Fig. 5. Diagram of a two-DOF robotic manipulator.

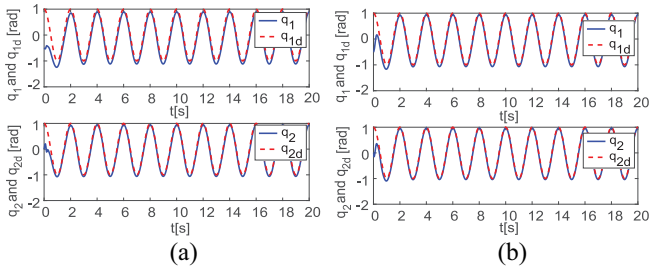

Fig. 6. Tracking performances. (a) Tracking performances with torque input (35). (b) Tracking performances with torque input (58).

Furthermore, the nonlinear system are stable under any initial conditions within finite time $t_\beta = t_3 + t_4$, where

$$t_3 = \frac{1}{(1-\iota)\varpi\alpha_2}\left(V\big(s_2(0), \tilde{W}(0)\big)^{1-\iota} - \left(\frac{\sigma_1}{(1-\varpi)\alpha_2}\right)^{\frac{(1-\iota)}{\iota}}\right)$$

$$t_4 = \max_{1\le i\le n}\left\{\frac{1}{\beta_i^{\frac{p}{q}}}\int_o^{|\varphi_i(t_0+t_3)|}\frac{1}{\left(\upsilon - \alpha_i^{-1}\upsilon^\gamma\right)^{\frac{p}{q}}}d\upsilon\right\} \tag{62}$$

where $\iota = (1/2)$, the period $t_\upsilon \in [t_0, t_3]$ is the reaching phase, and the period $t_\upsilon \in [t_3, t_4]$ is the sliding phase.

Proof: Because (60) is similar to (38), the proof in this section is similar to Theorem 1, which means the signals s_2, φ, $\dot{\varphi}$, and $\tilde{W}$ are semiglobally uniformly bounded and remain within the compact sets Ω_{s_2} Ω_{φ_2}, $\Omega_{\dot{\varphi}_2}$, and Ω_{w_2}. The prescribed constraints are satisfied under unknown initial conditions within finite time t_β. ■

IV. Simulation

To demonstrate the performance of the proposed finite-time control methods, the model of a two-joint manipulator in Fig. 5 is utilized for simulation. In this section, three parts are contained: 1) the proposed methods based on (35) and (58) are compared under the same conditions; 2) the proposed methods based on the novel sliding mode surfaces compared with other adaptive methods based on the existing sliding mode surface and BLFs; 3) the experiments on KINOVA robot. The parameters of robotic arm dynamics [5] are described as

$$M(q) = \begin{bmatrix} m_{11}(q) & m_{12}(q) \\ m_{21}(q) & m_{22}(q) \end{bmatrix} \tag{63}$$

where $m_{11}(q) = (1/2)m_1l_1^2 + m_2l_1^2 + (1/2)m_2l_2^2 + m_2l_1l_2\cos(q_2)$, $m_{12}(q) = (1/2)m_2l_2^2 + (1/2)m_2l_1l_2\cos(q_2)$, $m_{21}(q) = (1/2)m_2l_2^2 + (1/2)m_2l_1l_2\cos(q_2)$, and $m_{22}(q) = (1/2)m_2l_2^2$

$$C(q,\dot{q}) = \begin{bmatrix} c_{11}(q,\dot{q}) & c_{12}(q,\dot{q}) \\ c_{21}(q,\dot{q}) & c_{22}(q,\dot{q}) \end{bmatrix} \tag{64}$$

where $c_{12}(q,\dot{q}) = -(1/2)m_2l_1l_2(\dot{q}_1 + \dot{q}_2)\sin(q_2)$, $c_{11}(q,\dot{q}) = -(1/2)m_2l_1l_2\dot{q}_2\sin(q_2)$, $c_{21}(q,\dot{q}) = (1/2)m_2l_1l_2\dot{q}_1\sin(q_2)$, and $c_{22}(q,\dot{q}) = 0$

$$G(q) = \begin{bmatrix} g_1(q) \\ g_2(q) \end{bmatrix} \tag{65}$$

where $q = [q_1, q_2]^{\mathrm{T}}$, $\dot{q} = [\dot{q}_1, \dot{q}_2]^{\mathrm{T}}$, $\ddot{q} = [\ddot{q}_1, \ddot{q}_2]^{\mathrm{T}}$, $g_2(q) = (1/2)m_2l_2g\cos(q_1+q_2)$, $g_1(q) = ((1/2)m_1l_2 + m_2l_1)g\cos(q_1) + (1/2)m_2l_2g\cos(q_1+q_2)$, $m_1 = 2$ kg and $m_2 = 0.85$ kg are the masses of the robot arm links, $l_1 = 0.35$ m and $l_2 = 0.31$ m are the lengths of the robot arm links, and $g = 9.81$ m/s^2 is the gravity constant. We select $x_d = [\cos(\pi t), \cos(\pi t)]^{\mathrm{T}}$ as the desired trajectory.

The basis function NNs are utilized. Two hundred and fifty-six nodes are used for each basis function $S_i(X)$ with centers chosen in the area of $[-1,1]\times[-1,1]\times[-1,1]\times[-1,1]\times[-1,1]\times[-1,1]\times[-1,1]\times[-1,1]$, $\Gamma_1 = 100\mathrm{I}_{256\times256}$, $\Gamma_2 = 100\mathrm{I}_{256\times256}$, $\sigma_i = 0.002$, the initial weight are set as $\hat{W}_{1i} = 0$ and $\hat{W}_{2i} = 0$, $(i = 1, 2, \ldots, 256)$. In order to verify the compensation effort for input deadzone function, the unknown deadzone function is defined as $O_r(\tau) = \tau - b_r$ and $O_l(\tau) = 2(\tau - b_l)$, where $b_r = 4$ and $b_l = -2.5$.

A. NTSMC-Based Scheme and NFTSMC-Based Scheme

In this section, the simulation results need to satisfy the following objectives.

1) The proposed methods need less prior information, including initial state conditions, gain functions, and the width and slope of deadzone functions.
2) When input nonlinearities are considered, the output constraints are satisfied within the finite time T.
3) Compared with the proposed NN-based NTSMC, the proposed NN-based NFTSMC has faster convergence rate under the same conditions.

Choosing (35) and (58) as the control laws, the parameters of both schemes are chosen as $k_i = 0.4$, $\eta = 0.05$, $p_0 = 0.2$, $\mu_2 = 4$, $p = 7.5$, $q = 7$ and $\beta = \mathrm{diag}\{2, 3\}$. The preassigned time is selected as $T = 2$. The simulation about uncertain part ΔM is based on $\hat{m}_1 = 1.5$ kg and $\hat{m}_2 = 0.5$ kg. Compared with (35), the parameters of (58) are added with $\alpha = \mathrm{diag}\{1, 1\}$ and $\gamma = 1.7$ due to the additional item in $\alpha^{-1}\gamma\mathrm{sig}^{\gamma-1}(\varphi)\dot{\varphi}$. The initial states are selected as

$$q_1(0) = -0.5, q_2(0) = 0, \dot{q}_1(0) = 0, \dot{q}_2(0) = 0. \tag{66}$$

The results are presented in Figs. 6–8. The tracking performances are shown in Fig. 6(a) and (b). At these figures, all outputs track the desired trajectory successfully. Furthermore, in Fig. 6(b), the mean rate of convergence approximates 0.25 s. This observed value is notably inferior to the convergence rates corresponding to the trajectories delineated in Fig. 6(a), which are approximately 1.2 s and 0.47 s, respectively.

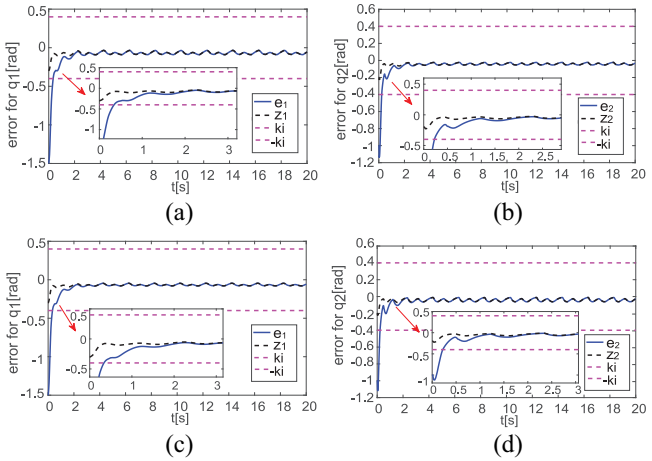

Fig. 7. Evolution of tracking errors and transformed tracking errors. (a) Evolution of e_1 and z_1 with torque input (35). (b) Evolution of e_2 and z_2 with torque input (35). (c) Evolution of e_1 and z_1 with torque input (58). (d) Evolution of e_2 and z_2 with torque input (58).

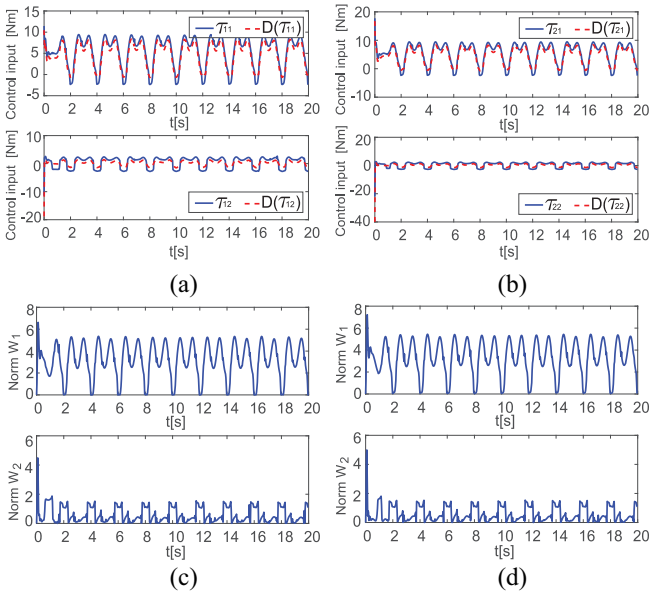

Fig. 8. Control inputs and norms of RBFNN. (a) Evolution of control inputs with torque input (35). (b) Evolution of control inputs with torque input (58). (c) Norms of NN weights with torque input (35). (d) Norms of NN weights with torque input (58).

The tracking errors are shown in Fig. 7(a)–(d). In Fig. 7(a)–(d), the output tracking errors convergence to a small neighborhood of zero within finite time. The tracking error signal e violates the prescribed constraints initially, but the transformed tracking error signal z satisfies it. Thus, the proposed sliding surfaces can be implemented under unknown initial conditions. The transformed error signal z is converted to the real tracking error e after the finite time T. The control input and norms of RBFNN are reflected in Fig. 8(a)–(d). Finally, in Fig. 8(c) and (d), the arguments of the unknown function remain within the compact set, on which the NN approximation is valid.

B. Numerical Comparison Between NFTSMC-Based Method and Other Existing SMC-Based Methods

In this section, we introduce the sliding-phase-based method and the reaching-phase-based method via barrier function without considering error-shifting function and chattering elimination. These methods are then further compared with the proposed NFTSMC-based method in this article.

The NFTSM surface for the sliding-phase-based method is chosen as $s_3 = \varphi_\alpha + \alpha^{-1}\text{sig}^{\gamma}(\varphi_\alpha) + \beta^{-1}\text{sig}^{(p/q)}(\dot{\varphi}_\alpha)$ and the following barrier function, $\varphi_{\alpha i}, i = 1, 2, \ldots, n$, is defined as $\varphi_{\alpha i} = (1/2)\ln(k^2/[k^2 - e_i^2])$. Therefore, the control law for the sliding-phase-based method is introduced as

$$\tau_\alpha = M_0\Bigg(B_2^{-1}\Bigg(-\eta_1\,\text{sign}(s_3) - \beta\frac{q}{p}\,\text{sig}^{2-\left(\frac{p}{q}\right)}(\dot{\varphi}_\alpha) - B_1 - \alpha^{-1}\gamma\,\text{sig}^{\gamma-1}(\varphi_\alpha)\beta\frac{q}{p}\,\text{sig}^{2-\left(\frac{p}{q}\right)}(\dot{\varphi}_\alpha)\Bigg) - B_4 + h\ddot{x}_d\Bigg) + \hat{W}^T S(X) \tag{67}$$

where $B_1 = [B_{11}, B_{12}, \ldots, B_{1n}] \in \mathbb{R}^n$, $B_{1i} = ([\dot{e}_i^2(e_i^2 + k^2)]/[(k^2 - e_i^2)^2])$, $i = 1, 2, \ldots, n$, $B_2 = \text{diag}\{B_{2i}\} \in \mathbb{R}^{n\times n}$, $B_{2i} = (e_i/[k^2 - e_i^2])$ and $B_4 = \mu_2\text{sign}(\text{B}_2)M_0^{-1}\text{sign}(\text{s}_3) \in \mathbb{R}^n$.

The control law for the reaching-phase-based method is similar to [16], [45] and chosen as

$$\tau_\beta = M_0\Bigg(-\alpha^{-1}\gamma\,\text{sig}^{\gamma-1}(e)\beta\frac{q}{p}\,\text{sig}^{2-\left(\frac{p}{q}\right)}(\dot{e}) - \eta_1 s_4 + \ddot{x}_d - \beta\frac{q}{p}\,\text{sig}^{2-\left(\frac{p}{q}\right)}(\dot{e})\Bigg) - \mu_2\,\text{sign}(\text{s}_4) + \hat{W}^T S(X) \tag{68}$$

where the NFTSM surface is $s_4 = e + \alpha^{-1}\text{sig}^{\gamma}(e) + \beta^{-1}\text{sig}^{(p/q)}(\dot{e})$.

The proposed schemes based on (58) and (67) are SGPFTS, and (68) is asymptotic convergence. The simulation results need to conform the following objectives.

1) The robotic system is SGPFTS. The convergence time is adjusted by parameters.
2) Solving the limitation of BLFs. The prescribed constraint is satisfied within finite time under unknown initial conditions.
3) Avoiding the uncertainty and indirectness caused by the reaching-phase-based methods.

The parameters of these three cases are chosen as, i.e., case 1 in (58): $\hat{m}_1 = 1.5$ kg, $\hat{m}_2 = 0.5$ kg, $\eta_1 = 0.05$, $\mu_2 = 4$, $p = 7.5$, $q = 6.5$, $\beta = \text{diag}\{2, 3\}$, $k = 0.2$, $\alpha = \text{diag}\{1, 1\}$, $\gamma = 1.7$, $p_0 = 0.01$, $T = 2$; case 2 in (67): $\hat{m}_1 = 1.5$ kg, $\hat{m}_2 = 0.5$ kg, $\eta_1 = 0.05$, $\mu_2 = 8$, $p = 7.5$, $q = 6.5$, $\beta = \text{diag}\{2, 3\}$, $\alpha = \text{diag}\{1, 1\}$, $\gamma = 1.7$, $k = 0.2$, $T = 2$; case 3 in (68): $\hat{m}_1 = 1.5$ kg, $\hat{m}_2 = 0.5$ kg, $\eta_1 = 0.05$, $p = 7.5$, $q = 6.5$, $\beta = \text{diag}\{2, 3\}$, $\alpha = \text{diag}\{1, 1\}$, $\gamma = 1.7$, $k = 1$, $\mu_2 = 5$.

The initial states of (58) and (68) are selected as

$$q_1(0) = -0.5, q_2(0) = -1, \dot{q}_1(0) = 0, \dot{q}_2(0) = 0. \tag{69}$$

The initial states of (67) are selected as

$$q_1(0) = 0.95, q_2(0) = 0.85, \dot{q}_1(0) = 0, \dot{q}_2(0) = 0. \tag{70}$$

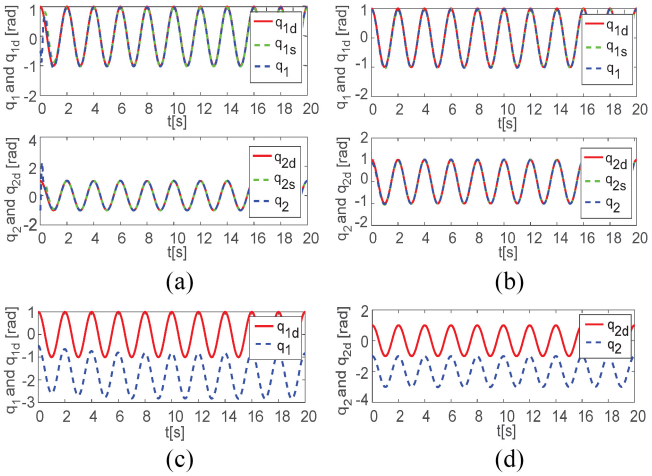

Fig. 9. Tracking performances. (a) Evolution with torque input (58). (b) Evolution with torque input (67). (c) Evolution of q_1 with torque input (68). (d) Evolution of q_2 with torque input (68).

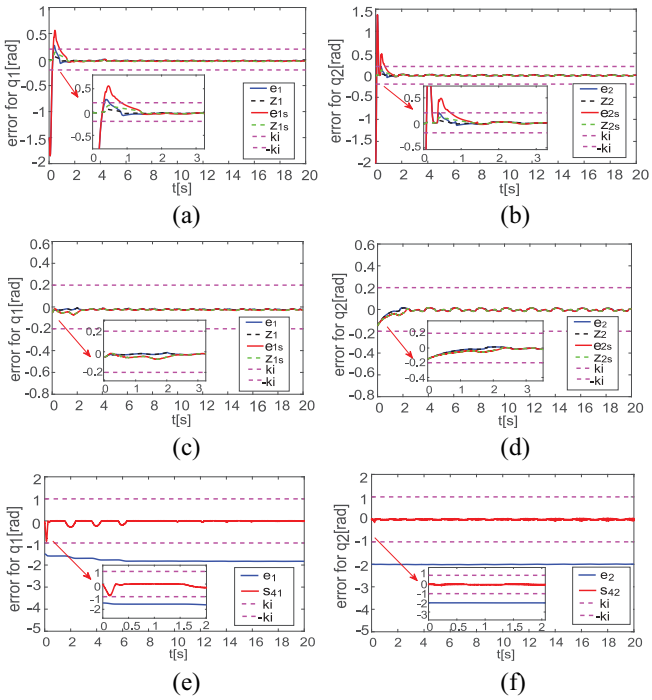

Fig. 10. Tracking errors. (a) Evolution of e_1 and z_1 with (58). (b) Evolution of e_2 and z_2 with (58). (c) Evolution of e_1 and z_1 with (67). (d) Evolution of e_2 and z_2 with (67). (e) Evolution of e_1 and z_1 with (68). (f) Evolution of e_2 and z_2 with (68).

In order to demonstrate that the convergence time is adjusted by parameters, the parameters of (58) and (67) are selected as $\gamma = 1.2$, which may receive a slower convergence rate than $\gamma = 1.7$. The other parameters are maintained.

The simulation results are shown in Figs. 9–11. In Fig. 9(a)–(d), all the desired trajectories are tracked successfully under the different tracking conditions. Compared with Fig. 9(a) and (b), the adaptive method based on asymptotic convergence has a wider range of tracking errors in Fig. 9(c) and (d) due to the indirect constraint.

The tracking errors are shown in Fig. 10(a) and (b). Fig. 10(a)–(d) (blue line and red line) show that the robotic

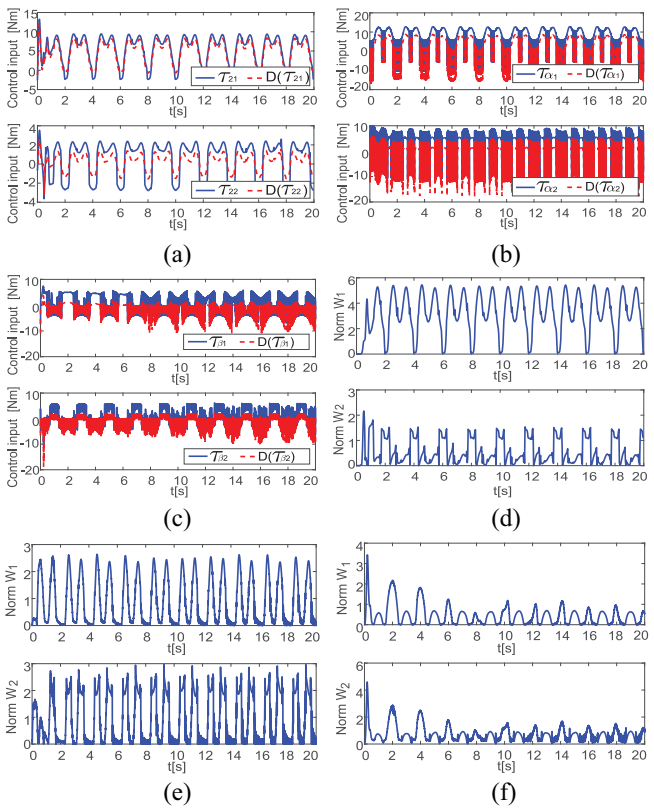

Fig. 11. Control inputs and norms of RBFNN. (a) Evolution of control inputs with (58). (b) Evolution of control inputs with (67). (c) Evolution of control inputs with (68). (d) Norms of NN weights with (58). (e) Norms of NN weights with (67). (f) Norms of NN weights with (68).

system is semi-global practical finite time stable and the convergence time can be adjusted by choosing suitable parameters. Compared with Fig. 10(c) and (d), the proposed method is still implemented successfully even if the prescribed constraint is violated initially. Thus, proposed method does not need initial state information of system, so the limitation of BLF is addressed. In reaching phase, the sliding vector s_4 is constrained directly instead of tracking errors e, and thus the tracking errors do not satisfy the prescribed constraint in Fig. 10(e) and (f).

The control inputs of the three adaptive methods are shown in Fig. 11(a)–(c). Compared with Fig. 11(b) and (c), the control inputs are continuous and bounded during the operation time, which addresses the chattering problem for SMC. Although the parameter $p_0 = 0.01$ in Section IV-B is more smaller than that in Section IV-A, the control objectives are still satisfied successfully, and thus the error-shifting function is suitable for all unknown initial condition cases. In Fig. 11(d)–(f), the norms of RBFNNs are remained in a compact set within finite time. Thus, the NN approximation is valid. In conclusion, the proposed schemes have better performances and need less prior information.

V. Experiment on KINOVA JACO2 Robot

KINOVA JACO2 robot platform has been performed to test the effectiveness of the proposed NN-based sliding control

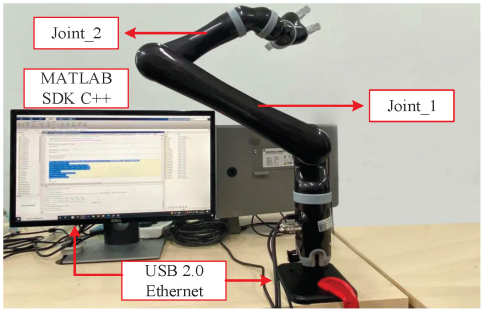

Fig. 12. Platform of KINOVA JACO2 robot.

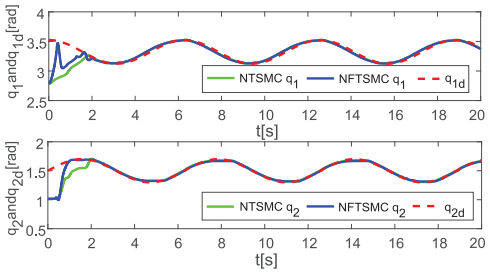

Fig. 13. Tracking performances of joint_1 and joint_2.

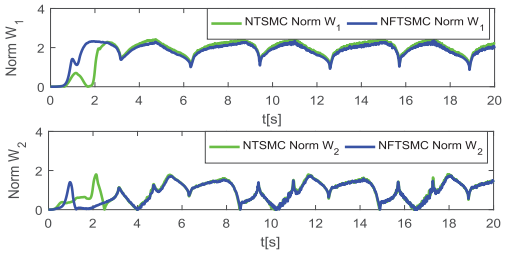

Fig. 14. Norms of NN weights of joint_1 and joint_2.

algorithm (35) and (58). In the experiment setup, as shown in Fig. 12, the KINOVA robot is six DOF curved wrist and each joint represents one DOF, which is connected with master computer through USB 2.0, Ethernet. The controller execution frequency is 100 Hz and the sampling frequency is 20 Hz. The program languages of the software development kit (SDK) is C++. The joint_1 and joint_2 are utilized to complete the trajectory tracking task under unknown initial conditions in this experiment.

In this experiment, the initial conditions of these two joint are set as: $q_1 = 2.8233$ rad, $q_2 = 1$ rad, $\dot{q}_1 = 0$ rad/s, and $\dot{q}_2 = 0$ rad/s. The desired trajectories of two joints are set as: 1) $q_{1d} = 3.3233 + 0.2\cos(t)$ and 2) $q_{2d} = 1.5000 + 0.2\sin(t)$. The key parameter is chosen as $p_0 = 0.1$ and others are similar to part A of this section.

The experiments results are shown in Figs. 13–16. In Fig. 13, both joints track the desired trajectories successfully and torque input (58) provides better-tracking performance. Fig. 14 shows the weights of NNs, which means that the NN approximations are valid. From Fig. 15, we can find that the tracking error e violates the prescribed constraints initially, but the transformed tracking error signal z satisfies it. Thus, the constraints for trajectory tracking task can be satisfied under

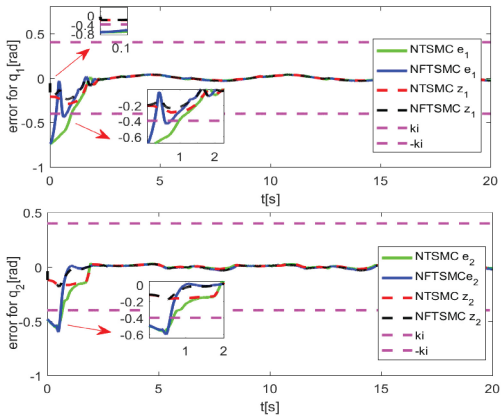

Fig. 15. Tracking errors of joint_1 and joint_2 with torque inputs (35) and (58).

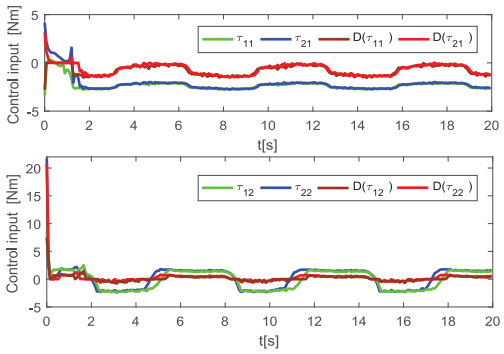

Fig. 16. Evolution of the torque inputs for joint_1 and joint_2 with (35) and (58).

unknown initial conditions. Fig. 16 is the description of the dynamic control torques of two joints.

Finally, despite the existence of uncontrollable factors, such as equipment instability, unknown deadzone functions, and unknown initial states, the experimental results can demonstrate that the proposed NN-based sliding mode schemes can track the desired trajectory and meet the prescribed constraints under unknown initial conditions in a robotic experiment environment.

VI. Conclusion

In this article, NN-based schemes have been proposed to address the tracking problems of a robotic manipulator with input deadzone and external disturbances. Less prior information is needed via novel NTSMC and NFTSMC with error-shifting function and barrier function. First, tracking errors satisfy the prescribed constraints under unknown initial conditions and further remain in the constraints after the preassigned time. Second, the prior knowledge of the robotic dynamics and nonlinearity functions are needless. Finally, the chattering phenomenon has been successfully reduced by introducing a mathematic technique in the switching law. There are good tracking performances in both simulation and experiment results. Fixed-time control scheme for unknown Euler-Lagrange system under unknown initial conditions need to be considered in further works.

REFERENCES

[1] K. Zhao, L. Chen, and C. P. Chen, "Event-based adaptive neural control of nonlinear systems with deferred constraint," *IEEE Trans. Syst., Man, Cybern., Syst.*, vol. 52, no. 10, pp. 6273–6282, Oct. 2022.

[2] L. Kong, W. He, Y. Dong, L. Cheng, C. Yang, and Z. Li, "Asymmetric bounded neural control for an uncertain robot by state feedback and output feedback," *IEEE Trans. Syst., Man, Cybern., Syst.*, vol. 51, no. 3, pp. 1735–1746, Mar. 2021.

[3] K. Zhao, L. Chen, W. Meng, and L. Zhao, "Unified mapping function-based neuroadaptive control of constrained uncertain robotic systems," *IEEE Trans. Cybern.*, vol. 53, no. 6, pp. 3665–3674, Jun. 2023.

[4] Y. Ouyang, L. Dong, L. Xue, and C. Sun, "Adaptive control based on neural networks for an uncertain 2-DoF helicopter system with input deadzone and output constraints," *IEEE/CAA J. Automatica Sinica*, vol. 6, no. 3, pp. 807–815, May 2019.

[5] W. He, A. O. David, Z. Yin, and C. Sun, "Neural network control of a robotic manipulator with input deadzone and output constraint," *IEEE Trans. Syst., Man, Cybern., Syst.*, vol. 46, no. 6, pp. 759–770, Jun. 2016.

[6] Y.-D. Song and S. Zhou, "Tracking control of uncertain nonlinear systems with deferred asymmetric time-varying full state constraints," *Automatica*, vol. 98, pp. 314–322, Dec. 2018.

[7] X. Yu, B. Li, W. He, Y. Feng, L. Cheng, and C. Silvestre, "Adaptive-constrained impedance control for human–robot co-transportation," *IEEE Trans. Cybern.*, vol. 52, no. 12, pp. 13237–13249, Dec. 2022.

[8] B. Yang, L. Cao, W. Xiao, D. Yao, and R. Lu, "Event-triggered adaptive neural control for multiagent systems with deferred state constraints," *J. Syst. Sci. Complexity*, vol. 35, no. 3, pp. 973–992, 2022.

[9] J. Liu, S. Vazquez, L. Wu, A. Marquez, H. Gao, and L. G. Franquelo, "Extended state observer-based sliding-mode control for three-phase power converters," *IEEE Trans. Ind. Electron.*, vol. 64, no. 1, pp. 22–31, Jan. 2017.

[10] L. Kong, J. Reis, W. He, and C. Silvestre, "Comprehensive nonlinear control strategy for VTOL-UAVs with windowed output constraints," *IEEE Trans. Control Syst. Technol.*, early access, Jul. 2023, doi: 10.1109/TCST.2023.3286044.

[11] J. Baek, M. Jin, and S. Han, "A new adaptive sliding-mode control scheme for application to robot manipulators," *IEEE Trans. Ind. Electron.*, vol. 63, no. 6, pp. 3628–3637, Jun. 2016.

[12] W. Qi, G. Zong, and H. R. Karimi, "Sliding mode control for nonlinear stochastic singular semi-Markov jump systems," *IEEE Trans. Autom. Control*, vol. 65, no. 1, pp. 361–368, Jan. 2020.

[13] C. Lin, "Nonsingular terminal sliding mode control of robot manipulators using fuzzy wavelet networks," *IEEE Trans. Fuzzy Syst.*, vol. 14, no. 6, pp. 849–859, Dec. 2006.

[14] S. S. Xu, C. Chen, and Z. Wu, "Study of nonsingular fast terminal sliding-mode fault-tolerant control," *IEEE Trans. Ind. Electron.*, vol. 62, no. 6, pp. 3906–3913, Jun. 2015.

[15] B. Xu, D. Zhou, and S. Sun, "Finite time sliding sector guidance law with acceleration saturation constraint," *IET Control Theory Appl.*, vol. 10, no. 7, pp. 789–799, 2016.

[16] Z. Chen, Q. Li, X. Ju, and F. Cen, "Barrier Lyapunov function-based sliding mode control for BWB aircraft with mismatched disturbances and output constraints," *IEEE Access*, vol. 7, pp. 175341–175352, 2019.

[17] M. Van, S. S. Ge, and H. Ren, "Robust fault-tolerant control for a class of second-order nonlinear systems using an adaptive third-order sliding mode control," *IEEE Trans. Syst., Man, Cybern., Syst.*, vol. 47, no. 2, pp. 221–228, Feb. 2017.

[18] H. Lee and V. I. Utkin, "Chattering suppression methods in sliding mode control systems," *Annu. Rev. Control*, vol. 31, no. 2, pp. 179–188, 2007.

[19] M. Gupta, S. Kumar, L. Behera, and V. K. Subramanian, "A novel vision-based tracking algorithm for a human-following mobile robot," *IEEE Trans. Syst., Man, Cybern., Syst.*, vol. 47, no. 7, pp. 1415–1427, Jul. 2017.

[20] Y. Feng, F. Han, and X. Yu, "Chattering free full-order sliding-mode control," *Automatica*, vol. 50, no. 4, pp. 1310–1314, 2014.

[21] W. Xu, Y. Jiang, and C. Mu, "Novel composite sliding mode control for PMSM drive system based on disturbance observer," *IEEE Trans. Appl. Supercond.*, vol. 26, no. 7, pp. 1–5, Oct. 2016.

[22] Z. Liu, Z. Han, Z. Zhao, and W. He, "Modeling and adaptive control for a spatial flexible spacecraft with unknown actuator failures," *Sci. China Inf. Sci.*, vol. 64, no. 5, pp. 1–16, 2021.

[23] W. He, X. Tang, T. Wang, and Z. Liu, "Trajectory tracking control for a three-dimensional flexible wing," *IEEE Trans. Control Syst. Technol.*, vol. 30, no. 5, pp. 2243–2250, Sep. 2022.

[24] H. Huang, W. He, Q. Fu, X. He, and C. Sun, "A bio-inspired flapping-wing robot with cambered wings and its application in autonomous airdrop," *IEEE/CAA J. Automatica Sinica*, vol. 9, no. 12, pp. 2138–2150, Dec. 2022.

[25] Z. Xu, Y. Kang, Y. Cao, and Z. Li, "Deep amended copert model for regional vehicle emission prediction," *Sci. China Inf. Sci.*, vol. 64, no. 3, 2021, Art. no. 139202.

[26] Q. Fu, J. Wang, L. Gong, J. Wang, and W. He, "Obstacle avoidance of flapping-wing air vehicles based on optical flow and fuzzy control," *Trans. Nanjing Univ. Aeronaut. Astron.*, vol. 38, no. 2, pp. 206–215, 2021.

[27] L. Kong, W. He, Z. Liu, X. Yu, and C. Silvestre, "Adaptive tracking control with global performance for output-constrained MIMO nonlinear systems," *IEEE Trans. Autom. Control*, vol. 68, no. 6, pp. 3760–3767, Jun. 2023, doi: 10.1109/TAC.2022.3201258.

[28] C. Yang, Y. Jiang, Z. Li, W. He, and C.-Y. Su, "Neural control of bimanual robots with guaranteed global stability and motion precision," *IEEE Trans. Ind. Informat.*, vol. 13, no. 3, pp. 1162–1171, Jun. 2017.

[29] C.-L. Hwang and L.-J. Chang, "Internet-based smart-space navigation of a car-like wheeled robot using fuzzy-neural adaptive control," *IEEE Trans. Fuzzy Syst.*, vol. 16, no. 5, pp. 1271–1284, Oct. 2008.

[30] W. He, B. Huang, Y. Dong, Z. Li, and C.-Y. Su, "Adaptive neural network control for robotic manipulators with unknown deadzone," *IEEE Trans. Cybern.*, vol. 48, no. 9, pp. 2670–2682, Sep. 2018.

[31] G. Peng, C. L. P. Chen, W. He, and C. Yang, "Neural-learning-based force sensorless admittance control for robots with input deadzone," *IEEE Trans. Ind. Electron.*, vol. 68, no. 6, pp. 5184–5196, Jun. 2021.

[32] H. Hu and P.-Y. Woo, "Fuzzy supervisory sliding-mode and neural-network control for robotic manipulators," *IEEE Trans. Ind. Electron.*, vol. 53, no. 3, pp. 929–940, Jun. 2006.

[33] J. Fei and C. Lu, "Adaptive sliding mode control of dynamic systems using double loop recurrent neural network structure," *IEEE Trans. Neural Netw. Learn. Syst.*, vol. 29, no. 4, pp. 1275–1286, Apr. 2018.

[34] S. M. Smaeilzadeh and M. Golestani, "Finite-time fault-tolerant adaptive robust control for a class of uncertain non-linear systems with saturation constraints using integral backstepping approach," *IET Control Theory Appl.*, vol. 12, no. 15, pp. 2109–2117, 2018.

[35] R. R. Selmic and F. L. Lewis, "Deadzone compensation in motion control systems using neural networks," *IEEE Trans. Autom. Control*, vol. 45, no. 4, pp. 602–613, Apr. 2000.

[36] L. Zhang, Y. Wang, Y. Hou, and H. Li, "Fixed-time sliding mode control for uncertain robot manipulators," *IEEE Access*, vol. 7, pp. 149750–149763, 2019.

[37] J. Campos and F. L. Lewis, "Deadzone compensation in discrete time using adaptive fuzzy logic," *IEEE Trans. Fuzzy Syst.*, vol. 7, no. 6, pp. 697–707, Dec. 1999.

[38] R. Sanner and J.-J. Slotine, "Gaussian networks for direct adaptive control," *IEEE Trans. Neural Netw.*, vol. 3, no. 6, pp. 837–863, Nov. 1992.

[39] F. Wang, B. Chen, C. Lin, J. Zhang, and X. Meng, "Adaptive neural network finite-time output feedback control of quantized nonlinear systems," *IEEE Trans. Cybern.*, vol. 48, no. 6, pp. 1839–1848, Jun. 2018.

[40] J. Zheng, H. Wang, Z. Man, J. Jin, and M. Fu, "Robust motion control of a linear motor Positioner using fast nonsingular terminal sliding mode," *IEEE/ASME Trans. Mechatronics*, vol. 20, no. 4, pp. 1743–1752, Aug. 2015.

[41] L. Kong, J. Reis, W. He, and C. Silvestre, "Experimental validation of a robust prescribed performance nonlinear controller for an unmanned aerial vehicle with unknown mass," *IEEE/ASME Trans. Mechatronics*, early access, Jul. 2023, doi: 10.1109/TMECH.2023.3282782.

[42] H. Zhang, A. Song, H. Li, and S. Shen, "Novel adaptive finite-time control of teleoperation system with time-varying delays and input saturation," *IEEE Trans. Cybern.*, vol. 51, no. 7, pp. 3724–3737, Jul. 2021.

[43] W. He, Y. Sun, Z. Yan, C. Yang, Z. Li, and O. Kaynak, "Disturbance observer-based neural network control of cooperative multiple manipulators with input saturation," *IEEE Trans. Neural Netw. Learn. Syst.*, vol. 31, no. 5, pp. 1735–1746, May 2020.

[44] B. Xu, "Robust adaptive neural control of flexible hypersonic flight vehicle with dead-zone input nonlinearity," *Nonlinear Dyn.*, vol. 80, no. 3, pp. 1509–1520, 2015.

[45] J. Long, S. Zhu, P. Cui, and Z. Liang, "Barrier Lyapunov function based sliding mode control for MARS atmospheric entry trajectory tracking with input saturation constraint," *Aerosp. Sci. Technol.*, vol. 106, Nov. 2020, Art. no. 106213.

Yu Zhang (Student Member, IEEE) received the M.Eng. degree in control engineering from the School of Intelligence Science and Technology, University of Science and Technology Beijing, Beijing, China, in 2022. He is currently pursuing the Ph.D. degree in computer science as a member of the Informatics 6-Chair of Robotics, Artificial Intelligence and Realtime Systems with the Technical University of Munich, Munich, Germany.

His current research interests include optimization and control in robotics, machine learning, adaptive and learning control.

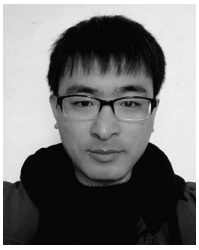

Linghuan Kong (Member, IEEE) received the M.Eng. degree from the School of Automation Engineering, University of Electronic Science and Technology of China, Chengdu, China, in 2019, and the Ph.D. degree from the School of Intelligence Science and Technology, University of Science and Technology Beijing, Beijing, China, in 2023.

He was a Research Assistant with the Faculty of Science and Technology, University of Macau, Macau, China, from September 2021 to October 2022. He is currently a Postdoctoral Fellow with the Faculty of Science and Technology, University of Macau. His current research interests include robotics, unmanned aerial vehicles, and adaptive and learning control.

Shuang Zhang (Member, IEEE) received the Ph.D. degree in control science and engineering from the Department of Electrical and Computer Engineering, National University of Singapore, Singapore, in 2012.

She is currently an Associate Professor with the School of Automation and Electrical Engineering, University of Science and Technology Beijing, Beijing, China. Her current research interests include robotics, adaptive controls, and vibration controls.

Xinbo Yu (Member, IEEE) received the B.E. degree in control technology and instrument and the Ph.D. degree in control science and engineering from the School of Automation and Electrical Engineering, University of Science and Technology Beijing, Beijing, China, in 2013 and 2020, respectively.

He is currently working as an Associate Professor with the Institute of Artificial Intelligence, University of Science and Technology Beijing. His current research interests include adaptive NNs control, robotics and human–robot interaction, intelligent robot control, and human–robot collaboration.

Yu Liu (Senior Member, IEEE) received the Ph.D. degree in automatic control from the South China University of Technology, Guangzhou, China, in 2009.

He was a visiting student with the Department of Mechanical Engineering, Concordia University, Montreal, QC, Canada, from 2008 to 2009, and a Visiting Scholar with the Department of Electrical and Computer Engineering, University of Nebraska–Lincoln, Lincoln, NE, USA, from 2017 to 2018. He is currently a Professor with the School of Automation Science and Engineering, South China University of Technology, and with the Research and Development Center of Precision Electronic Manufacturing Technology, Guangzhou Institute of Modern Industrial Technology, Guangzhou. His current research interests include distributed parameter systems, flexible systems, robotic, adaptive learning control, and machine vision.